ACS APPLIED MATERIALS & INTERFACES

Research Article

www.acsami.org

High-Active Anatase TiO_2 Nanosheets Exposed with 95% {100} Facets Toward Efficient H_2 Evolution and CO_2 Photoreduction

Hua Xu,[†,‡,§] Shuxin Ouyang,*[,‡] Peng Li,[†,‡,§] Tetsuya Kako,[†,‡] and Jinhua Ye*[,†,‡,§,∥]

[†]Graduate School of Chemical Science and Engineering, Hokkaido University, Sapporo 060-0814, Japan

[‡]Environmental Remediation Materials Unit and [§]International Center for Materials Nanoarchitectonics (WPI-MANA), National Institute for Materials Science (NIMS), 1-1 Namiki, Tsukuba 305-0044, Japan

[∥]TU-NIMS Joint Research Center, School of Materials Science and Engineering, Tianjin University, 92 Weijin Road, Nankai District, Tianjin 300072, P.R. China

Supporting Information

ABSTRACT: We succeed in preparation of anatase TiO_2 single crystals with marked photocatalytic activity via a facile and effective method. This TiO_2 is composed of TiO_2 ultrathin nanosheets (2 nm in thickness) with 95% of exposed {100} facet, which is considered to be the active facet for photocatalytic reaction. This percentage (95%) is the highest among previously reported {100} facet exposed anatase TiO_2. More importantly, due to this high ratio, our developed TiO_2 nanosheets showed marked photocatalytic activity, about 5 times higher activity in both H_2 evolution and CO_2 reduction than the reference sample, TiO_2 cuboids with 53% of exposed {100} facet. For the TiO_2 nanosheets, both the higher percentage of exposed {100} facets and larger surface area can offer more surface active sites in the photocatalytic reaction. On the other hand, the superior electronic band structure which results from the higher percentage of {100} facet is also beneficial for the higher activity. This study exemplifies that the facet engineering of semiconductors is one of the most effective strategies to achieve advanced properties over photofunctional materials for solar energy conversion.

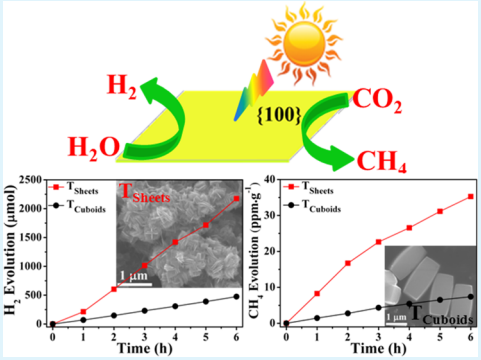

KEYWORDS: *anatase TiO_2, nanosheets, {100} facet, surface chemistry, photocatalysis*

1. INTRODUCTION

Photocatalysis is well-considered to be a potential solution to the worldwide energy shortage and environmental pollution, such as CO_2 photoreduction into solar fuels, photocatalytic water splitting into H_2, and photodegradation of organic pollutants.[1−4] For a photocatalyst, the photocatalytic performance is largely dependent on the surface structure because many physical and chemical processes take place on the surface.[3−5] In the case of anatase TiO_2, among the most investigated {101}, {001}, and {100} facets, the {100} facet is considered to be the most active facet in the photocatalysis because of its superior surface atomic structure and electronic structure.[6,7] On the {100} surface, 100% Ti atoms are 5-coordinated Ti (Ti_{5c}), these under-coordinated Ti atoms (Ti_{5c}) can act as active sites in the photocatalytic reaction, which is beneficial for the higher photocatalytic activity.[8] In parallel, it is reported that TiO_2 sample with more {100} facet exposed owns a superior electronic band structure, in which more strongly reductive electrons can be generated on the conduction band and then transferred to the TiO_2 surface to reduce H^+ into H_2, resulting in a higher photocatalytic activity in the H_2 evolution.[7,9] Thereby, fabrication of TiO_2 single crystals exposed with more active {100} facets will be an effective way to optimize the photocatalytic properties of anatase TiO_2 and then find its promising application in the field of renewable energy, such as H_2 evolution and photoreduction of CO_2 in hydrocarbon fuels (e.g. CH_4).

However, based on the Wulff construction and theoretically calculated surface energy ({101} (0.44 J/m^2) < {100} (0.53 J/m^2) < {001} (0.90 J/m^2)), due to the minimization of surface energy during the crystal growth, the anatase TiO_2 under equilibrium condition are dominated by the thermodynamically stable {101} facets (up to 94%) and few {001} facets, no {100} facets will appear.[10,11] In order to obtain the TiO_2 single crystals exposed with {100} facets, many efforts have been carried out. In the first beginning, Barnard et al. theoretically predicted that the {100} facet would appear as the "belt" at the center of anatase particles (Scheme 1), and it can be experimentally obtained in the water-terminated surfaces and hydrogen-poor surfaces (especially for the oxygenated surfaces).[12] Those predictions paved the road for chemists to experimentally realize the fine tuning of the particle morphology via controlling the surface chemistry. After that, several studies have confirmed that anatase TiO_2 single crystals

Received: November 8, 2012
Accepted: January 28, 2013
Published: January 29, 2013

Scheme 1. Schematic Illustration of Anatase TiO_2 Single Crystals Exposed with Different Crystal Facets

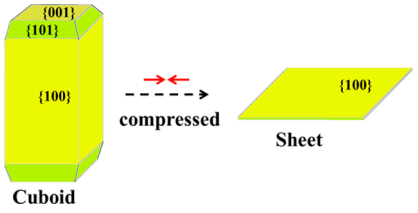

with dominant {100} facets were experimentally prepared in the morphology of rods or cuboids.[7,9,13] Nevertheless, there are still some problems for those reported TiO_2 cuboids, which limited their practical application. For those TiO_2 particles, besides the {100} facet, other facets (such as {001} and {101} facets) on the upper and bottom of the cuboids will be also exposed (Scheme 1). Up to now, the highest percentage of the {100} facet exposed on TiO_2 cuboids is reported to be 85.7%, and the TiO_2 cuboids exhibited a relatively small surface area of 5.8 m^2/g.[13] As we all know, surface area plays an important role in the photocatalytic reaction, which is not only beneficial for the adsorption of the reactant but also can offer more active sites for the photoreaction.[14,15] Therefore, in order to largely enhance the photocatalytic activity, both the percentage of the exposed {100} facets and surface area should be increased for the anatase TiO_2.

As shown in Scheme 1, we hypothesize that if we reduce the thickness of the TiO_2 cuboids in the [100] direction to some extent, ultrathin TiO_2 nanosheets will be obtained. In this case, the percentages of the {101} and {001} facets will be significantly decreased, resulting in a larger percentage of {100} facets being exposed. Accordingly, we adopt a facile and effective method to fabricate the ultrathin anatase TiO_2 nanosheets with both a high percentage of the {100} facet exposed (up to 95%) and large surface area (57.1 m^2/g). To the best of our knowledge, both the percentage of the {100} facet exposed and the surface area of our prepared TiO_2 nanosheets reported in this work are the highest so far. Due to the high ratio of {100} facets exposed as well as the larger surface area, which can offer more active sites in the phtocatalytic reaction, our developed TiO_2 nanosheets showed marked photocatalytic activity, about 5 times higher activity in both of H_2 evolution and CO_2 photoreduction than the reference sample, TiO_2 cuboids with 53% of exposed {100} facet. Moreover, the superior electronic band structure that results from the higher percentage of exposed {100} facet on the TiO_2 nanosheets also makes a great contribution to the higher photocatalytic activity.

2. EXPERIMENTAL SECTION

Materials Synthesis. All chemicals were of analytical grade and used as received without further purification. In a typical synthesis of the TiO_2 nanosheets, 1 mmol of TiF_4 was firstly dissolved into 2 mL of ethanol. Then, 30 mL of benzyl alcohol containing 3 mmol of oleic acid was added in the above solution. After being treated at 200 °C for 40 min, the final TiO_2 powders can be obtained. In order to remove the surface adsorbed organics and fluorine, the TiO_2 powders were calcined at 600 °C for 2 h. The final obtained TiO_2 nanosheets with clean surfaces are denoted as T_{Sheets}. The photocatalytic properties of the TiO_2 sample before and after calcination are discussed in the Supporting Information (Figure S1–S3).

Meanwhile, TiO_2 cuboids with less {100} facets exposed were also prepared in comparison to the 95% of {100} facets exposed TiO_2 nanosheets. The TiO_2 cuboids were synthesized following the method reported by Pan et al. via reacting 32 mg of $TiOSO_4$ in 40 mL of HF solution (40 mM) at 180 °C for 2 h, then calcining at 600 °C for 2 h to remove the surface fluorine.[7] The obtained TiO_2 cuboids with clean surfaces are denoted as $T_{Cuboids}$.

Characterizations. X-ray diffraction patterns were recorded on a Rigaku Multiflex diffractometer (RINT 2000; Rigaku Corp. Japan) with monochromatized Cu Ka radiation (λ = 1.54178 Å). The size and morphology of the samples were observed by a scanning electron microscope (SEM, JSM-6701F, JEOL Co., Japan) and transmission electron microscope (TEM, JEM-200 CX, JEOL) operating at 200 kV. The Brunauer–Emmett–Teller (BET) surface areas were deducted by a surface area analyser (BEL Sorp-II mini, BEL Japan Co., Japan) with nitrogen absorption at 77 K. Raman measurement was carried out using Raman spectroscopy (NRS-1000; Jasco Corp. Japan). UV-visible absorption spectra were measured on a UV-visible spectrophotometer (UV-2500 PC, Shimadzu Co., Japan). X-ray photoelectron spectroscopy (XPS) was conducted on Thermo ESCALAB250 using monochromatized Al Ka at $h\upsilon$ = 1486.6 eV. The binding energies were calibrated to the C1s peak by 284.6 eV. The electron paramagnetic resonance (EPR) spectra were measured to confirm the presence of oxygen vacancy on JEOL JES-FA200 Electron Spin Resonance Spectrometer at ambient temperature. The CO_2 pulse chemisorption tests were carried out on Micromeritics Autochem II Chemisorption Analyzer at 35 °C with a fixed volume loop of 0.05 mL.

Photocatalytic H_2 Evolution. The photocatalytic reactions of H_2 evolution were carried out in a closed gas circulation system with an external-irradiation type of a glass reactor. The light source was a 300 W Xenon arc lamp. The intensity of the light at 300–800 nm was measured to be 240 mW/cm^2 by using a spectroradiometer (USR-40; Ushio Inc., Japan). The co-catalyst Pt was loaded by an in-situ photodeposition method. The 1 wt % of Pt-loaded catalyst (60 mg) was dispersed with a magnetic stirrer in a methanol aqueous solution (50 mL of CH_3OH and 220 mL of H_2O). The evolved gas including H_2 was analyzed using an online gas chromatograph (GC-8A; Shimadzu) equipped with a thermal conductivity detector (TCD).

CO_2 Photoreduction. In the photocatalytic reduction of CO_2, 40 mg of the sample without any cocatalyst was uniformly dispersed on a glass reactor with a base area of 8.1 cm^2. A 300 W Xenon arc lamp was used as the light source for the photocatalytic reaction. The volume of the reaction system was around 390 mL. The reaction setup was vacuum treated several times, and then high-purity CO_2 gas was introduced into the reaction system to achieve a pressure of 80 kPa. Deionized water (3 mL) was injected into the reaction system. During the irradiation, about 0.5 mL of gas was taken from the reaction cell at given intervals for subsequent CH_4 concentration analysis using a gas chromatograph (GC-14B, Shimadzu) equipped with a flame ionized detector (FID) and methanizer.

3. RESULTS AND DISCUSSION

The powder XRD patterns of the prepared TiO_2 nanosheets and cuboids are shown in Figure 1. The XRD profiles of the two TiO_2 samples can coincidently be indexed to the pure anatase TiO_2 with tetragonal structure (space group $I4_1/amd$, $a = b$ = 3.782 Å, c = 9.502 Å, JCPDS card 73-1764). The peaks at 25.25, 37.72, 48.03, 53.91, and 54.99° can be assigned to (101),

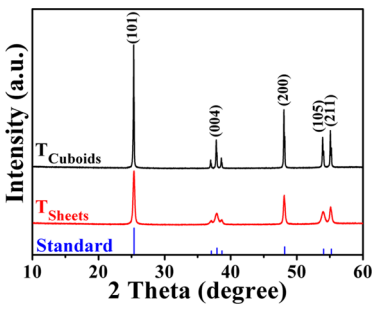

Figure 1. XRD patterns of TiO_2 nanosheets and cuboids.

dx.doi.org/10.1021/am302631b | ACS Appl. Mater. Interfaces 2013, 5, 1348–1354

(004), (200), (105), and (211) crystal planes of anatase TiO_2, respectively. The values of the full width at half maximum (FWHM) at 25.25, 37.72, and 48.03° (indexed to be (101), (004), and (200) crystal planes, respectively) are measured to be 0.11, 0.26, and 0.09 for $T_{Cuboids}$ and 0.32, 0.68, and 0.23 for T_{Sheets}, respectively. It is obvious that $T_{Cuboids}$ exhibits better crystallinity than T_{Sheets}. Moreover, according to the JCPDS standard card, the peak intensity of $I_{(101)}$:$I_{(004)}$:$I_{(200)}$ equals 100:18:23; it is noteworthy that the relative peak intensities of the (101), (004), and (200) planes are calculated to be 100:23:48 and 100:20:53 for $T_{Cuboids}$ and T_{Sheets}, respectively, indicating that both $T_{Cuboids}$ and T_{Sheets} have the preferential crystallographic orientation along the [100] direction.

The morphology of the TiO_2 nanosheets was observed by SEM. As shown in Figure 2a, the TiO_2 sample consists of large

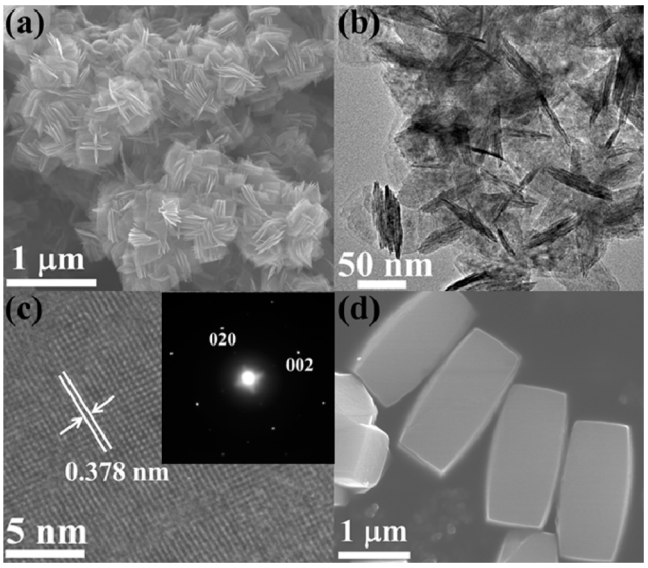

Figure 2. SEM image (a), TEM image (b), HRTEM image (c), and SAED pattern (inset of c) of the TiO_2 nanosheets, as well as the SEM image of the TiO_2 cuboids (d).

amounts of paperlike nanosheets. These nanosheets assemble together to form the hierarchical architectures. In order to observe the nanosheets clearly, the TEM image is shown in Figure 2b. Those sheets are around 70 nm × 70 nm in size with a thickness around 2 nm. The high-resolution TEM image (Figure 2c) shows that the distance of the visible lattice fringes over a large area was measured to be 0.378 nm, which is in agreement with the lattice spacing of (010) atomic plane of anatase TiO_2.[16] Furthermore, the selected-area electron diffraction (SAED) pattern (inset of Figure 2c) can be indexed to the diffraction spots of the [100] zone for the TiO_2 single crystalline, indicating that our prepared T_{Sheets} are exposed with the {100} facet. This result is in agreement with the analysis of the XRD pattern, which implies that the T_{Sheets} preferential crystallographic growth is along the [100] direction. In addition, the low-magnification SEM image (Supporting Information Figure S4) proved that our prepared TiO_2 sample is composed of almost all the nanosheets. Hence, based on the above information, we can calculate that the percentage of the exposed {100} facet in T_{Sheets} is about 95%. (The calculation method is shown in the Supporting Information.) The morphology of the TiO_2 cuboids can be observed as shown in Figure 2d. The cuboids are 0.6 μm × 1.5 μm with a thickness of about 300 nm. The percentage of the exposed {100} facet in $T_{Cuboids}$ was reported to be 53%.[7] In addition, with the decrease of the thickness from 300 nm (cuboids) to 2 nm (nanosheets), the surface areas are largely increased from 3.9 m^2/g for $T_{Cuboids}$ to 57.1 m^2/g for T_{Sheets} (Supporting Information Figure S5). Both the higher percentage of {100} facets and larger surface area of our developed T_{Sheets} can offer more active sites in the photocatalytic reaction, which are beneficial for photocatalytic performance.

Meanwhile, the crystal structures of the two TiO_2 samples were also investigated by Raman spectroscopy. As shown in Figure 3, the peaks appearing at 396, 515, and 638 cm^{-1} of the

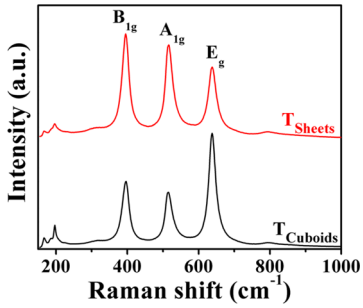

Figure 3. Raman spectra of the TiO_2 nanosheets and cuboids exposed with different percentage of {100} facets.

two TiO_2 samples correspond to the B_{1g}, A_{1g}, and E_g peaks of anatase TiO_2, respectively.[17] However, the relative intensities of the three peaks in the two TiO_2 samples are obviously different, in which the intensities of the A_{1g} and B_{1g} peaks of T_{Sheets} are obviously much higher than that of $T_{Cuboids}$. For anatase TiO_2, the E_g, B_{1g}, and A_{1g} peaks are mainly related to the symmetric stretching vibration, symmetric bending vibration, and antisymmetric bending vibration of the O−Ti−O, respectively.[17] The slab models of the {100} and {101} surfaces are shown in Figure 4. It can be observed that the {101} surface is

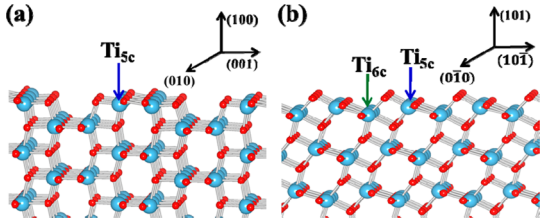

Figure 4. Slab models of {100} surface (a) and {101} surface (b) of anatase TiO_2. (Ti_{5c}: 5-coordinated Ti atoms. Ti_{6c}: fully or 6-coordinated Ti atoms).

flatter than the {100} surface and 100% Ti atoms on the top layer of the {100} surface are 5-coordinated, thus it can be deduced that more O−Ti−O bonding on the {100} surface is bending vibration because of its unique atomic arrangement.[17] For $T_{Cuboids}$, it was composed of 53% {100}, 33% {101}, and 14% {001} facets.[7] In comparison to T_{Sheets} with up to 95% {100} facet, the bending vibration of the O−Ti−O will be much stronger on the T_{Sheets}. Therefore, the relative peaks in 396 and 515 cm^{-1} for T_{Sheets} are much higher than that of $T_{Cuboids}$.

The UV−visible absorption spectra of the TiO_2 nanosheets and cuboids are shown in Figure 5a. Compared with the $T_{Cuboids}$ exposed with 53% {100} facet, the intrinsic absorption

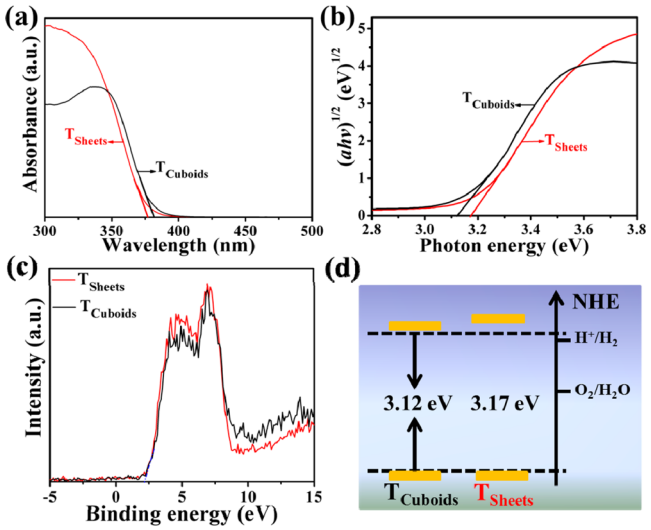

Figure 5. UV−visible absorption spectra (a), the corresponding plots of transformed Kubelka−Munk function versus the energy of photon (b), valence band XPS spectra of the TiO_2 nanosheets and cuboids exposed with different percentages of {100} facets (c), and schematic illustration of the band structures of the two TiO_2 samples (d).

edge of our prepared T_{Sheets} with 95% {100} facets has an obvious blue-shift by 5 nm. On the basis of the formula $a = B_i(h\nu - E_g)^2/h\nu$ (a is the absorption coefficient, $h\nu$ is the incident photon energy, and B_i is the absorption constant for indirect transitions),[18] the band gaps are deduced to be 3.12 and 3.17 eV for the $T_{Cuboids}$ and T_{Sheets}, respectively (Figure 5b). The valence band maximum of the two TiO_2 samples are measured to be similar (Figure 5c), thus the larger band gap of the T_{Sheets} is indicated to a higher conduction band minimum of the T_{Sheets} in contrast to the $T_{Cuboids}$ (Figure 5d). Our experimental phenomenon is in agreement with the previous report. It is well-accepted that the {100} facet owns superior electronic structure in comparison with other facets (e.g. {001} facet and {101} facet), and TiO_2 single crystals exposed with more {100} facets will exhibit higher conduction band minimum.[7−9,19] In this work, when the percentage of the {100} facet is increased from 53% to 95%, the conduction band minimum of the T_{Sheets} obviously increases. The higher conduction band minimum, on which more reductive electrons can be generated and then transferred to the TiO_2 surface to take part in the photocatalytic reaction, is beneficial for the photocatalytic reaction.[8,20]

As a photocatalyst, anatase TiO_2 has a conduction band edge that is more negative [vs normal hydrogen electrode (NHE)] than the H^+/H_2 reduction potential; thus, the TiO_2 can efficiently split water into hydrogen, which is a promising candidate as a future energy carrier.[21] So, herein, the H_2 evolution tests in the presence of methanol as hole scavenger were carried out to evaluate the photocatalytic activity of the prepared T_{Sheets} and $T_{Cuboids}$. As shown in Scheme 2a, when the TiO_2 is excited by the light, the photogenerated electrons will move to the conduction band, leaving a positive hole in the valence band. In the H_2 evolution, the electrons will then transfer to the TiO_2 surface on the Pt sites to reduce H^+ into H_2; the holes will be exhausted via oxidizing the sacrifice reagent (methanol) to prevent the hole-electron recombination.[1] As shown in Figure 6a, the H_2 evolution rates over 6 h are measured to be 362 and 79 μmol·h^{-1} for the T_{Sheets} and

Scheme 2. Schematic Illustration of H_2 Evolution (a) and CO_2 Photoreduction (b) Processes

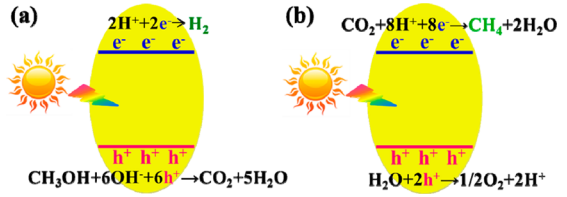

$T_{Cuboids}$, respectively; the photocatalytic activity of T_{Sheets} is 4.6 times higher than that of $T_{Cuboids}$.

In general, the photocatalytic activity is affected by various factors, such as optical absorption properties, crystallinity, surface area, facet reactivity, and defect contents, and so on.[1,22,23] Herein, the effect of several factors on the photocatalytic activity are discussed as following. First, considering the optical absorption properties, the more photons that are absorbed by the TiO_2 photocatalyst, the more photoexcited charge carriers can be produced to take part in the photocatalytic reaction.[24] As shown in Figure 5a, $T_{Cuboids}$ exhibits red-shifted optical absorption edge in comparison to T_{Sheets}, while the intensity of the absorption of T_{Sheets} is higher than $T_{Cuboids}$ in the region of 300−350 nm. Hence, their photocatalytic performance under monochromatic light centered at a wavelength of 361 nm was studied. In this case, $T_{Cuboids}$ obviously absorbs more light than T_{Sheets} (Supporting Information Figure S6a); however, the activity of T_{Sheets} is 3.3 times higher than that of $T_{Cuboids}$ as shown in Supporting Information Figure S6b. Next, let us discuss the effect of crystallinity; obviously, $T_{Cuboids}$ has better crystallinity than T_{Sheets} (Figure 1), which is beneficial for the inhibition of charge recombination in the photocatalytic reaction,[25] but T_{Sheets} still exhibits significantly higher photocatalytic activity than $T_{Cuboids}$. Thus, the effect of both optical absorption properties and crystallinity will not be the reason for the higher activity of T_{Sheets}.

Then, taking the surface area into account, TiO_2 with a larger surface area can not only offer more active reaction sites on the surface but also is beneficial for the reactant adsorption.[26,27] In comparison to $T_{Cuboids}$ (3.9 m^2/g), T_{Sheets} exhibits a relatively large surface area of 57.1 m^2/g. With a larger surface area of the T_{Sheets}, the surface area of the exposed {100} facet will be also increased, thus more 5-coordinated Ti atoms (Ti_{5c}) will exist on the surface. Experimentally, we compared the photocatalytic activity of the two TiO_2 samples in the same total surface area as shown in Figure 6b. In this case, the activity of T_{Sheets} (362 μmol h^{-1}) is about 3.5 times that of $T_{Cuboids}$ (104 μmol h^{-1}); in contrast to the 4.6 times higher activity of T_{Sheets} than $T_{Cuboids}$ with the same mass but different surface area, the above control experiments indicate that the surface area indeed makes contributions to the enhancement of photocatalytic activity; however, some other factors (including facet reactivity, surface defects, and electronic band structures) might be also contributing to the higher photocatalytic activity.

Surface chemistry (such as facet reactivity and surface defects) always plays important roles in the photocatalysis.[23,28] The {100} facet is reported to be the active facet in H_2 evolution because of its superior surface properties.[7] With more {100} facets exposed on T_{Sheets}, more 5-coordinated Ti atoms can be offered on the surface to act as active sites for the photocatalytic reaction. Meanwhile, because of the largely

dx.doi.org/10.1021/am302631b | ACS Appl. Mater. Interfaces 2013, 5, 1348−1354

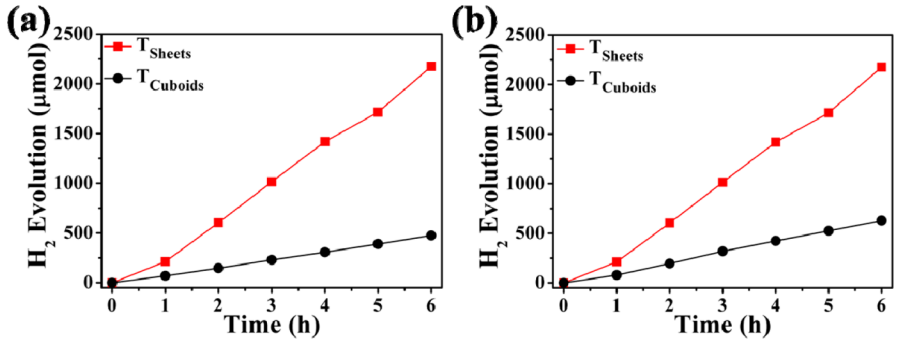

Figure 6. (a) Photocatalytic H_2 evolution tests of the 1 wt % Pt-loaded TiO_2 samples with the same mass of 60 mg under UV-visible light irradiation (λ > 300 nm). (b) Comparison of photocatalytic activities between T_{Sheets} (60 mg × 57.1 m^2/g = 3.43 m^2) and $T_{Cuboids}$ (879 mg × 3.9 m^2/g = 3.43 m^2) with same total surface area (ca. 3.43 m^2) under UV−visible light irradiation (λ > 300 nm).

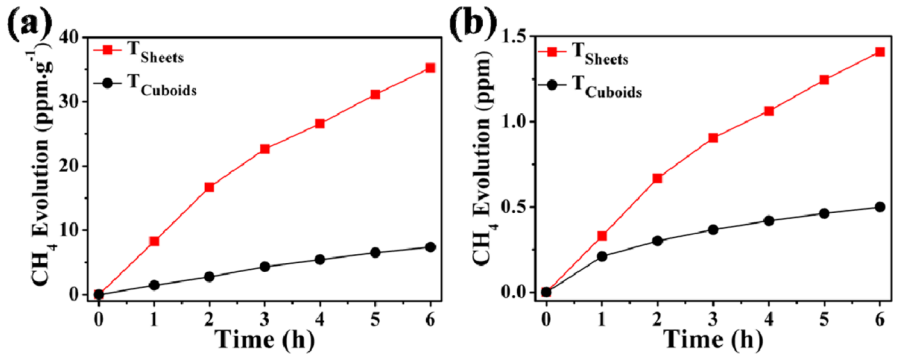

Figure 7. (a) Photocatalytic CO_2 photoreduction tests of the TiO_2 samples without any cocatalyst under UV−visible light irradiation (λ > 300 nm). (b) Comparison of photocatalytic activities between T_{Sheets} (40 mg × 57.1 m^2/g = 2.28 m^2) and $T_{Cuboids}$ (585 mg × 3.9 m^2/g = 2.28 m^2) with same total surface area (ca. 2.28 m^2) under UV−visible light irradiation (λ > 300 nm).

undercoordinated Ti and O atoms existing on the {100} surface (Figure 4), our previous theoretical-calculation results revealed that the oxygen vacancy is more easily produced on the {100} surface than it is on the {101} surface.[29] Herein, more {100} facet is exposed on T_{Sheets} than on $T_{Cuboids}$ based on the analysis of Raman spectra, thus greater oxygen vacancy might be formed on the surface of T_{Sheets}. To check the existence of the oxygen vacancies on the TiO_2 surface, the electron paramagnetic resonance (EPR) spectra were adopted as shown in Supporting Information Figure S7. The signal observed at g = 2.002 for T_{Sheets} is characteristic of a paramagnetic Ti^{3+} existing on the surface of TiO_2.[30] T_{Sheets} shows an EPR signal at g = 2.002, but $T_{Cuboids}$ does not, indicating that some oxygen vacancy exists on the T_{Sheets} surface. Those oxygen vacancies are known to act as active reaction sites in the photocatalytic reaction.[3,29] In addition, the CO_2 pulse chemisorption results showed that T_{Sheets} can adsorb 0.15 mL/g CO_2 but the CO_2 adsorption property of $T_{Cuboids}$ is very weak (Supporting Information Figure S8 and Table S1). The CO_2 chemisorption over T_{Sheets} results from its surface oxygen vacancy,[31,32] which is further confirmation that oxygen vacancies are produced on the surface of T_{Sheets}. Finally, besides its superior surface atomic structure, the {100} facet also exhibits excellent surface electronic structure. Herein, with more {100} facet exposed in our developed T_{Sheets}, the electronic band gap of T_{Sheets} is increased. As shown in Figure 5d, the conduction band minimum of T_{Sheets} is much higher than that of $T_{Cuboids}$, the superior electronic band structure of the T_{Sheets} will make a great contribution to the enhanced photocatalytic activity, in which more strongly reductive electrons can be produced then transferred to the surface to reduce H^+ into H_2.[7,8,19]

On the basis of the above analysis, we can conclude that the higher percentage of the exposed {100} facet (up to 95%) and the larger surface area (57.1 m^2/g) make more {100} facets exposed on the T_{Sheets} surface; accordingly, oxygen vacancies together with more Ti_{5c} atoms exist on the surface to act as active reaction sites, and the superior electronic band structure is also beneficial for the photocatalytic reaction, followed with a higher photocatalytic activity of T_{Sheets}.

Furthermore, the photocatalytic CO_2 reduction into hydrocarbon fuels is another promising application for TiO_2 photocatalyst.[20] The direct reduction of CO_2 into hydrocarbon fuels (e.g. CH_4) using solar energy is one of the best strategies to manage both global warming and the energy shortage.[33−36] In the CO_2 photoreduction process, as shown in Scheme 2b, the photogenerated holes in the valence band oxidize water into hydrogen ions (H^+) via the half-reaction $H_2O + 2h^+ \rightarrow 1/2O_2 + 2H^+$, and the photogenerated electrons in the conduction band reduce CO_2 to CH_4 via the reaction of $CO_2 + 8H^+ + 8e^- \rightarrow CH_4 + 2H_2O$.[37] Here, the photocatalytic activity of the TiO_2 nanosheets and cuboids in CO_2 photoreduction were evaluated over 40 mg of photocatalyst without any cocatalyst in a gas−solid system as shown in Figure 7a. Besides CH_4 as the main product, trace amounts of CO can also be detected. The CH_4 evolution rates over T_{Sheets} and $T_{Cuboids}$ are determined to be 5.8 and 1.2 ppm·g^{-1}·h^{-1}, respectively; in which T_{Sheets} is 4.8 times higher than $T_{Cuboids}$. The photoreactivity order is the same as that of the H_2 evolution test, T_{Sheets} > $T_{Cuboids}$. When comparing the photocatalytic activity of the two TiO_2 samples in the same

total surface area, as shown in Figure 7b, T_{Sheets} still exhibits higher photocatalytic activity, about 2.8 times that of $T_{Cuboids}$. Herein, the reason for the higher activity of T_{Sheets} in CO_2 photoreduction is similar to that in H_2 evolution. Firstly, both the oxygen vacancy existing on the TiO_2 surface and the larger surface area of TiO_2 nanosheets are beneficial for the CO_2 adsorption. Then, the photoexcited electrons on the conduction band of TiO_2 transfer to the TiO_2 surface to reduce CO_2 into CH_4. During this reaction process, since more {100} facet is exposed on the surface of T_{Sheets}, more surface active sites (such as Ti_{5c} atoms) will be offered. On the other hand, T_{Sheets} exhibits a higher conduction band minimum (Figure 5d), on which more reductive electrons can be generated; the more the reductive potential of the electrons, the higher the CH_4 output efficiency. Thus, the higher photocatalytic activity of T_{Sheets} is ascribed to its larger surface area, more active sites (e.g. oxygen vacancy and Ti_{5c} atoms) existing on the surface, and the superior electronic band structure. Moreover, controlled experiments show that no CH_4 was evolved when the photocatalytic reaction was carried out in the dark or irradiated in the absence of photocatalyst, revealing that the reduction of CO_2 is driven by light irradiation over the photocatalyst.

4. CONCLUSION

Ultrathin anatase TiO_2 nanosheets exposed with 95% of {100} facets are prepared. In contrast to the reference sample, TiO_2 cuboids exposed with 53% of {100} facets, our developed TiO_2 nanosheets have a relatively higher percentage of exposed {100} facet, larger surface area, and superior electronic band structure, which means that the TiO_2 nanosheets exhibit significantly higher photocatalytic activity in terms of both H_2 evolution and CO_2 photoreduction processes. This study is related to the fine-tuning of the TiO_2 photocatalyst exposed with a high percentage of active facets for excellent photocatalytic performance in the potential application of renewable energy. Furthermore, the present work also motivates us to process the facet engineering of other functional materials to achieve advanced and excellent properties over photocatalysts.

■ ASSOCIATED CONTENT

Supporting Information

Calculation of the percentage of exposed crystal facets, study of the photocatalytic properties related to the surface reconstruction over TiO_2 nanosheets, low magnification SEM image, N_2 adsorption−desorption isotherms, comparison study of H_2 evolution, EPR spectra, and CO_2 pulse chemisorption tests. This material is available free of charge via the Internet at http://pubs.acs.org.

■ AUTHOR INFORMATION

Corresponding Author

*Tel.: 81-29-859-2646. E-mail: Jinhua.YE@nims.go.jp (J.Y.); OUYANG.Shuxin@nims.go.jp (S.O.).

Notes

The authors declare no competing financial interest.

■ ACKNOWLEDGMENTS

This work was partially supported by World Premier International (WPI) Research Center Initiative on Materials Nanoarchitectonics (MANA).

■ REFERENCES

(1) Tong, H.; Ouyang, S. X.; Bi, Y. P.; Umezawa, N.; Oshikiri, M.; Ye, J. H. *Adv. Mater.* **2012**, *24*, 229−251.
(2) Tang, J. W.; Zou, Z. G.; Ye, J. H. *Angew. Chem. Int. Ed.* **2004**, *43*, 4463−4466.
(3) Bi, Y. P.; Ouyang, S. X.; Umezawa, N.; Cao, J. Y.; Ye, J. H. *J. Am. Chem. Soc.* **2011**, *133*, 6490−6493.
(4) Jiang, J.; Zhao, K.; Xiao, X. Y.; Zhang, L. Z. *J. Am. Chem. Soc.* **2012**, *134*, 4473−4476.
(5) Wang, X. N.; Huang, B. B.; Wang, Z. Y.; Qin, X. Y.; Zhang, X. Y.; Dai, Y.; Whangbo, M. H. *Chem.—Eur. J.* **2010**, *16*, 7106−7109.
(6) Anatase TiO_2 is in the tetragonal structure and belonging to the space group of $I4_1/amd$, in which $a = b = 3.782$ Å, $c = 9.502$ Å, thus the {100} facet is equal to the {010} facet in anatase TiO_2.
(7) Pan, J.; Liu, G.; Lu, G. M.; Cheng, H. M. *Angew. Chem. Int. Ed.* **2011**, *50*, 2133−2137.
(8) Liu, G.; Yu, J. C.; Lu, G. Q.; Cheng, H. M. *Chem. Commun.* **2011**, *47*, 6763−6783.
(9) Pan, J.; Wu, X.; Wang, L. Z.; Liu, G.; Lub, G. Q.; Cheng, H. M. *Chem. Commun.* **2011**, *47*, 8361−8363.
(10) Lazzeri, M.; Vittadini, A.; Selloni, A. *Phys. Rev. B:Condens. Matter* **2001**, *63*, 155409.
(11) Lazzeri, M.; Vittadini, A.; Selloni, A. *Phys. Rev. B:Condens. Matter* **2002**, *65*, 119901.
(12) Barnard, A. S.; Curtiss, L. A. *Nano Lett.* **2005**, *5*, 1261−1266.
(13) Zhao, X. W.; Jin, W. Z.; Cai, J. G.; Ye, J. F.; Li, Z. H.; Ma, Y. R.; Xie, J. L.; Qi, L. M. *Adv. Funct. Mater.* **2011**, *21*, 3554−3563.
(14) Chen, X. Q.; Li, Z. S.; Ye, J. H.; Zou, Z. G. *Chem. Mater.* **2010**, *22*, 3583−3585.
(15) Xu, H.; Zhang, L. Z. *J. Phys. Chem. C* **2010**, *114*, 940−946.
(16) In the JCPDS standard card, the *d*-spacing of the (010) crystal plane is not recorded. However, the lattice parameter for anatase TiO_2 is $a = b = 3.782$ Å, $c = 9.502$ Å, thus we can deduce that the lattice spacing of the (010) crystal plane is 0.378 nm.
(17) Tian, F.; Zhang, Y. P.; Zhang, J.; Pan, C. X. *J. Phys. Chem. C* **2012**, *116*, 7515−7519.
(18) Butler, M. A. *J. Appl. Phys.* **1977**, *48*, 1914−1920.
(19) Liu, G.; Sun, C. H.; Yang, H. G.; Smith, S. C.; Wang, L. Z.; Lu, G. Q.; Cheng, H. M. *Chem. Commun.* **2010**, *46*, 755−757.
(20) Inoue, T.; Fujishima, A.; Konishi, S.; Honda, K. *Nature* **1979**, *277*, 637−638.
(21) Fujishima, A.; Honda, K. *Nature* **1972**, *238*, 37−38.
(22) Hoffmann, M. R.; Martin, S. T.; Choi, W. Y.; Bahnemann, D. W. *Chem. Rev.* **1995**, *95*, 69−96.
(23) Linsebigler, A. L.; Lu, G. Q.; Yates, J. T. *Chem. Rev.* **1995**, *95*, 735−758.
(24) Xu, H.; Chen, X. Q.; Ouyang, S. X.; Kako, T.; Ye, J. H. *J. Phys. Chem. C* **2012**, *116*, 3833−3839.
(25) Ouyang, S. X.; Ye, J. H. *J. Am. Chem. Soc.* **2011**, *133*, 7757−7763.
(26) Li, Y. Z.; Sun, Q.; Kong, M.; Shi, W. Q.; Huang, J. C.; Tang, J. W.; Zhao, X. J. *J. Phys. Chem. C* **2011**, *115*, 14050−14057.
(27) Fan, X. X.; Wang, Y.; Chen, X. Y.; Gao, L.; Luo, W. J.; Yuan, Y. P.; Li, Z. S.; Yu, T.; Zhu, J. H.; Zou, Z. G. *Chem. Mater.* **2010**, *22*, 1276−1278.
(28) Yang, H. G.; Sun, C. H.; Qiao, S. Z.; Zou, J.; Liu, G.; Smith, S. C.; Cheng, H. M.; Lu, G. Q. *Nature* **2008**, *453*, 638−641.
(29) Xu, H.; Reunchan, P.; Ouyang, S. X.; Tong, H.; Umezawa, N.; Kako, T.; Ye, J. H. *Chem. Mater.* **2013**, DOI: 10.1021/cm303502b.
(30) Anpo, M.; Che, M.; Fubini, B.; Garrone, E.; Giamello, E.; Paganini, M. C. *Top. Catal.* **1999**, *8*, 189−198.
(31) Thompson, T. L.; Diwald, O.; Yates, J. T. *J. Phys. Chem. B* **2003**, *107*, 11700−11704.
(32) Thompson, T. L.; Yates, J. T. *Top. Catal.* **2005**, *35*, 197−209.
(33) Cheng, H. F.; Huang, B. B.; Liu, Y. Y.; Wang, Z. Y.; Qin, X. Y.; Zhang, X. Y.; Dai, Y. *Chem. Commun.* **2012**, *48*, 9729−9731.
(34) Li, P.; Ouyang, S. X.; Xi, G. C.; Kako, T.; Ye, J. H. *J. Phys. Chem. C* **2012**, *116*, 7621−7628.

(35) Zhou, Y.; Tian, Z. P.; Zhao, Z. Y.; Liu, Q.; Kou, J. H.; Chen, X. Y.; Gao, J.; Yan, S. C.; Zou, Z. G. *ACS Appl. Mater. Interfaces* **2011**, *3*, 3594−3601.
(36) Chen, X. Y.; Zhou, Y.; Liu, Q.; Li, Z. D.; Liu, J. G.; Zou, Z. G. *ACS Appl. Mater. Interfaces* **2012**, *4*, 3372−3377.
(37) Xi, G. C.; Ouyang, S. X.; Ye, J. H. *Chem.—Eur. J.* **2011**, *17*, 9057−9061.